European Polymer Journal 242 (2026) 114413

Contents lists available at ScienceDirect

European Polymer Journal

journal homepage: www.elsevier.com/locate/europolj

Precision ring-opening metathesis polymerization of synergistic ethylhexyl norbornene dicarboximide copolymers: unraveling side chain-thermal behavior correlations

Mohammed F. Radwan [a,b,*], Mohamed E. Abdu [a,c], Mahmoud Z. Basyouni [a,d], Mostafa M. Elkady [e], Hiroshi Furuno [f], Andrew M. Spring [a,**]

[a] Department of Interdisciplinary Engineering Sciences, Chemistry and Materials Science, Interdisciplinary Graduate School of Engineering Sciences, Kyushu University, 6-1 Kasuga-koen, Fukuoka 816-8580, Japan
[b] Department of Chemistry, Faculty of Science, South Valley University, Qena 83523, Egypt
[c] Department of Chemistry, Faculty of Science, Zagazig University, Zagazig 44519, Egypt
[d] Department of Chemistry, Faculty of Science, Benha University, Benha 13518, Egypt
[e] Interdisciplinary Graduate School of Engineering Sciences, Kyushu University, 6-1 Kasuga-Koen, Kasuga, Fukuoka 816-8580, Japan
[f] Department of Internationalization and Future Conception, Faculty of Engineering Sciences, Kyushu University, 6-1 Kasuga-koen, Kasuga, Fukuoka 816-8580, Japan

ARTICLE INFO

Keywords:
Norbornene polymers. Tunable architectures
Living polymerization
Catalyst efficiency
Functional copolymers
and Thermal robustness

ABSTRACT

Norbornene-derived polymers represent a versatile platform in advanced materials due to their tunable molecular architectures; however, unsubstituted norbornene dicarboximides (NDI) often suffer from poor solubility, limited stability, and restricted control during polymerization. To address these challenges, we designed well-defined norbornene-based homo- and copolymers incorporating ethylhexyl substituents *via* ring-opening metathesis polymerization (ROMP), achieving a balance between rigidity and flexibility. Polymerization behavior was systematically examined under living conditions by monitoring conversion, initiator-to-monomer ratios, and the efficiency of Grubbs catalysts (G1, HG1, HG2, G3, G2), with G1 providing superior control and narrow dispersities (PDI) Furthermore, a series of random copolymers (P1–P6) bearing diverse functional groups was synthesized and characterized by FT-IR, FESEM, GPC (PDI = 1.15–1.24) and NMR spectroscopy, with further analysis for P4 *via* ^{19}F-NMR. Thermal studies revealed high decomposition (358–459 °C) and glass transition (80-168 °C) temperatures, strongly influenced by sidechain identity and connectivity to the norbornene core. The optical characteristics were evaluated with a wide optical bandgap (3.53–4.53 eV). These findings demonstrate that the present norbornene dicarboximide frameworks thus combine excellent thermal robustness with high optical transparency, establishing them as promising high-performance materials for advanced applications.

1. Introduction

Ruthenium-catalyzed ring-opening metathesis polymerization (ROMP) has become a key technique in polymer synthesis, offering precise control over molecular weight and dispersity [1–4]. It enables the formation of varied architectures, including homopolymers, copolymers, brushes, star and ladder structures, yielding materials from soft elastomers to rigid thermoplastics and cross-linked networks [5–10]. Driven by the release of ring strain in cyclic olefins, especially norbornene derivatives, ROMP provides high efficiency, suppresses side reactions, and allows the design of functional polymers with tailored structural and physical properties [11–15].

Norbornene and its derivatives are key in polymer chemistry due to their significant ring strain (~27 kcal/mol), enabling efficient ROMP and compatibility with diverse functional groups [16]. Since Asrar's initial synthesis in 1992 *via* Diels-Alder reactions, their nitrogen atoms have offered versatile sites for chemical modification [17]. This enables the production of high-molecular-weight polymers with controlled architectures and minimal side [18–20]. Poly(norbornene dicarboximide) (poly-NDI) exemplifies this class, combining thermal stability,

* Corresponding author at: Department of Interdisciplinary Engineering Sciences, Chemistry and Materials Science, Interdisciplinary Graduate School of Engineering Sciences, Kyushu University, 6-1 Kasuga-koen, Fukuoka 816-8580, Japan.
** Corresponding author.
E-mail addresses: mohammedfouadali51@sci.svu.edu.eg (M.F. Radwan), spring.mark.andrew.284@m.kyushu-u.ac.jp (A.M. Spring).

https://doi.org/10.1016/j.eurpolymj.2025.114413
Received 29 September 2025; Received in revised form 19 November 2025; Accepted 22 November 2025
Available online 24 November 2025

mechanical strength, optical transparency, low moisture uptake, and excellent film-forming properties, supporting applications in drug delivery [21], energy storage [22–24], membrane gas separation [25–30], optoelectronics [31,32], and capacitors [33,34]. Besides their established utility in ROMP, norbornene dicarboximide derivatives also act as effective monomers in vinyl-addition polymerization, producing saturated backbones with excellent thermal and oxidative stability [35,36]. Although mechanistically distinct, this route further demonstrates the versatility of the norbornene framework for developing high-performance polymers with adjustable structural and physical properties [37–39].

Unsubstituted norbornene dicarboximide suffers from poor solubility, mechanical fragility, and limited reactive sites, restricting post-polymerization modifications and practical applications [40,41]. Functionalized derivatives address these limitations by enhancing solubility, enabling structural characterization, and allowing tailored properties for advanced polymer systems. Recent studies demonstrated their versatility: *trans*-poly-NDIs with chromophore units exhibit strong electro-optic responses [42], chlorophenyl-substituted polymers support flexible OLEDs [43], homo- and copolymers enable gas separation [44], photocrosslinkable block copolymers show improved thermal and dielectric properties [45], and post-functionalized polymers form micelles for efficient drug encapsulation [46,47], copolymers with tetraphenylethylene units enabled selective aniline sensing [48], highlighting the broad applicability of norbornene-based materials.

The integration of norbornene and ethylhexyl functionalities within a single polymer framework yields a synergistic effect that balances the intrinsic limitations of each unit. While polymers derived exclusively from norbornene exhibit high rigidity and excellent thermal stability [49], their unsubstituted form suffers from poor solubility, thereby restricting their applicability in film formation and solution-based processing [50]. Conversely, polymers containing ethylhexyl side chains offer superior solubility and flexibility but typically suffer from reduced thermal endurance, especially for polymers containing ethylhexyl moieties as additives or plasticizing agents [51–54]. By combining both groups along the backbone, a synergistic balance emerges, yielding polymers that maintain processability and solubility while preserving thermal robustness and mechanical strength, enabling advanced high-performance material development.

Building upon this concept, the present study introduces the *N*-ethylhexyl norbornene dicarboximide (Et-Hex-NDI) monomer and establishes a comprehensive approach to the ring-opening metathesis polymerization (ROMP) process. This strategy enabled precise monitoring of monomer-to-polymer conversion, ultimately confirming complete monomer consumption within 36 min and providing critical insights into the underlying polymerization kinetics. Special attention is given to the living nature of the ROMP process, explored across a range of repeating units defined by varying monomer-to-initiator feed ratios (n = 50–300) and evaluating different Grubbs initiator generations, The data demonstrated that the first-generation Grubbs initiator (G1) exhibited optimal performance with the highly strained norbornene backbone, consistently affording polymers with controlled molecular weight and low dispersity. Beyond the development of homopolymers, this study expanded the scope to synthesize a set of copolymers (P1–P6) by copolymerizing Et-Hex-NDI with a series of norbornene derivatives bearing either aromatic (phenothiazine, carbazole, phenyl, and pentafluorophenyl) or aliphatic (adamantyl and cyclohexyl) pendant groups. These copolymers displayed considerable diversity in their thermophysical properties, as demonstrated by thermogravimetric (TGA) and differential scanning calorimetry (DSC). All samples displayed high thermal stability, with decomposition temperatures ranging from 358 °C to 459 °C and glass transition temperatures between 86 °C and 168 °C. Furthermore, optical characterization revealed absorption onset wavelengths ranging from 274 nm to 351 nm, corresponding to optical band gaps of 3.53 eV to 4.53 eV, thereby classifying these materials as wide-bandgap polymers. Based on these results, the norbornene dicarboximide copolymers demonstrate remarkable thermal stability coupled with wide optical band gaps that absorb predominantly in the near-UV region, affording visible transparency and effective UV shielding. Such attributes position them as promising candidates for optically clear films, protective coatings, LEDs, electronic encapsulation, and electro-optic devices demanding durability and optical precision.

2. Experimental Section

2.1. Synthesis of precursors and comonomers

The synthesis and characterization of the precursor *exo*-norbornene-5,6-dicarboxylic anhydride (*exo*-NDA, **1**; **Scheme S1** and **Fig. S1**) is outlined in the Supporting Information. The phenothiazine-functionalized norbornene-5,6-dicarboximide (PT-NDI) and carbazole-functionalized norbornene-5,6-dicarboximide (Cbz-NDI) monomers were obtained following procedures described in our earlier work [55,56]. Moreover, the preparation of *N*-pentafluorophenyl- (F_5Ph-NDI), *N*-cyclohexyl- (Cy-Hex-NDI), *N*-phenyl- (Ph-NDI), and *N*-adamantyl-substituted (Adm-NDI) norbornene-5,6-dicarboximide derivatives was carried out following previously reported methodologies [57–59].

2.2. Preparation of N-ethylhexyl norbornene-5,6-dicarboximide (Et-Hex-NDI) monomer

It was prepared according to our previous work [60]. A solution of *exo*-NDA **1** (10.0 g, 0.061 mol) in chloroform (100 mL) was prepared and heated to reflux. Subsequently, 2-ethylhexylamine (7.87 g, 0.061 mol) was introduced gradually under reflux conditions. The reaction mixture was kept at reflux for 24 h to ensure complete conversion. Upon completion, the solvent was removed under reduced pressure using a rotary evaporator. The resulting crude material was subjected to purification by column chromatography employing a 10:90 mixture of tetrahydrofuran and hexane as the eluent. This process yielded a transparent oily product, which was further dried under vacuum at 70 °C for 12 h, affording the desired compound as a clear oil (11.9 g) in 71 % isolated yield. LRMS (EI +) calculated for $C_{17}H_{25}NO_2$: *m/z* 275.19; determined *m/z* 275.00. Elemental analysis; calculated; C, 74.14; H, 9.15; N, 5.09; O, 11.62; found; C, 74.13; H, 9.14; N, 5.08; O, 11.64. ^{1}H-NMR (400 MHz, $CDCl_3$) δ: 6.26 (t, J = 1.8 Hz, 2H), 3.37–3.31 (m, 2H), 3.25 (t, J = 1.6 Hz, 2H), 2.65 (d, J = 1.3 Hz, 2H), 1.70–1.65 (m, 1H), 1.50–1.14 (m, 10*H*), 0.87–0.84 (m, 6H); ^{13}C NMR (151 MHz, $CDCl_3$) δ: 178.49, 178.48, 137.89, 47.84, 45.23, 42.85, 42.61, 37.81, 30.58, 28.48, 23.98, 23.04, 14.11, 10.41, Fig. 1. Also, **Fig. S2 (A-E)** showed EI-MS and ^{13}C-, COSY, DEPT, and HMQC-NMR spectra of the monomer.

2.3. Tracking monomer-to-polymer conversion

Poly(Et-Hex-NDI) was synthesized by distributing 100 mg of monomer into nine Radley's Carousel reactor vessels under an inert atmosphere, each dissolved in 1 mL anhydrous chloroform and stirred for 30 min for complete dissolution, followed by rapid initiation with a G1 initiator solution (5.98 mg, 7.26×10^{-6} mol) in 0.3 mL dry chloroform. The reaction progress was terminated at specific times: 1, 3, 6, 12, 24, 36, 48, 60, and 90 min, by adding 3 mL of ethyl vinyl ether (EVE) and stirring for 2 h. Solvent and excess EVE were then removed under reduced pressure, and the obtained polymers were analyzed by ^{1}H NMR and GPC to assess monomer conversion.

2.4. Preparation of poly(Et-Hex-NDI) homopolymers at varied monomer-to-initiator feed ratios

Homopolymerization of Et-Hex–NDI was conducted under a dry nitrogen atmosphere, where six reaction vessels each contained 150 mg (5.45×10^{-4} mol) of the monomer dissolved in anhydrous chloroform (2

mL) and stirred at room temperature for 30 min to achieve homogeneity. Separate G1 initiator solutions were prepared, adjusting catalyst loadings to attain the desired monomer-to-initiator ratios of: n = 50 (8.97 mg, 1.09×10^{-5} mol), n = 100 (4.48 mg, 5.45×10^{-6} mol), n = 150 (2.99 mg, 3.63×10^{-6} mol), n = 200 (2.24 mg, 2.72×10^{-6} mol), n = 250 (1.79 mg, 2.18×10^{-6} mol), and n = 300 (1.49 mg, 1.82×10^{-6} mol), where is the (n) is the number of repeating units. Each catalyst solution (0.2 mL, dry chloroform) was swiftly added to the monomer solution to initiate polymerization, which proceeded for 36 min at room temperature before quenching with 3 mL of EVE. The mixtures were maintained for 2 h to ensure complete termination, then purified by repeated chloroform dissolution and methanol precipitation to remove residual catalyst. The purified poly(Et-Hex-NDI) samples were collected by filtration, dried in a vacuum at 40 °C for 12 h, and obtained in yields of 61 %, 72 %, 83 %, 73 %, 77 %, and 52 %, respectively, for the six targeted ratios. The corresponding ^{1}H-NMR spectral data of the homopolymer at the ratios (n = 100 – 300) are presented in **Fig. S3** and **Table S1**.

2.5. Effect of Grubbs catalyst initiators on the polymerization of the Et-Hex-NDI monomer

The polymerization of Et-Hex-NDI was performed in four independent reactions under a nitrogen atmosphere to evaluate the effect of different Grubbs-type initiators on ROMP efficiency. Each reaction used 150 mg of monomer (5.45×10^{-4} mol) dissolved in 2 mL of anhydrous chloroform and stirred at room temperature for 30 min before catalyst addition. Separate solutions of Hoveyda–Grubbs first-generation (HG1, 6.54 mg), Hoveyda–Grubbs second-generation (HG2, 6.83 mg), Grubbs third-generation (G3, 9.64 mg), and Grubbs second-generation (G2, 9.25 mg) were prepared in 0.2 mL of dry chloroform, each corresponding to 1.09×10^{-6} mol of active species. The catalyst solutions were immediately introduced into the monomer solutions and proceeded at ambient temperature for 36 min before quenching with 3 mL of EVE. After stirring for an additional 2 h, the resulting polymers were precipitated into methanol, washed thoroughly, and dried under vacuum at 40 °C for 12 h, affording off-white solids in 86 % (HG1), 97 % (HG2), 79 % (G3), and 89 % (G2) yields. The corresponding ^{1}H NMR spectral data are presented in **Fig. S4** and **Table S2**.

2.6. Synthesis of copolymers

To obtain the desired molecular weights for each copolymer composition, the corresponding monomer and initiator quantities were precisely calculated based on their molar ratios (**Table S3**). Copolymerizations were performed by combining an equal mass portion (100 mg each) of the Et-Hex-NDI monomer and the respective comonomer, such as PT-NDI, Cbz-NDI, Ph-NDI, F_5Ph-NDI, Adm-NDI, or Cy-Hex-NDI, under a nitrogen atmosphere. The mixtures were dissolved in 2 mL of dry chloroform and stirred at room temperature for 15 min to ensure uniformity. Separately, G1 initiator solutions were prepared in 0.2 mL of degassed chloroform, with respective quantities for each reaction: 4.47 mg (5.44×10^{-6} mol), 4.68 mg (5.68×10^{-6} mol), 6.40 mg (7.77×10^{-6} mol), 5.44 mg (6.62×10^{-6} mol), 5.75 mg (6.98×10^{-6} mol), and 6.32 mg (7.68×10^{-6} mol), respectively. Each catalyst solution was promptly introduced into the corresponding monomer mixture, maintained at room temperature for 36 min, and quenched with EVE. After 2 h of post-quenching stirring, solvents were evaporated, and the crude polymers were purified by repeated chloroform–methanol precipitation and vacuum-dried at 40 °C for 12 h to obtain white solids.

(a) Poly(Et-Hex/PT – NDI) copolymer 1 (P1)

Following the established copolymerization methodology, phenothiazine-substituted-NDI (PT-NDI) was employed as the comonomer. The reaction afforded (150 mg) of product as an off-white crystalline material, representing an isolated yield of 75 %. The ^{1}H NMR spectrum (400 MHz, $CDCl_3$) displayed δ values at 7.13 (q, J = 7.6 Hz, 4H), 6.92 (d, J = 7.8 Hz, 4H), 5.61 (dd, J = 89.9, 7.1 Hz, 4H), 4.40 (t, J = 6.2 Hz, 2H), 4.12 (s, 2H), 3.72 (s, 2H), 3.33 (s, 4H), 2.96 (t, J = 11.4 Hz, 4H), 2.65–2.59 (m, 4H), 2.14–2.09 (m, 2H), 1.65 (d, J = 57.2 Hz, 4H), 1.24 (t, J = 6.6 Hz, 9H), 0.87 (t, J = 6.4 Hz, 6H).

(b) Poly(Et-Hex/Cbz – NDI) copolymer 2 (P2)

Following the established copolymerization methodology, carbazole-substituted-NDI (Cbz-NDI) was employed as the comonomer. The reaction afforded (137 mg) of product as an off-white crystalline material, representing an isolated yield of 69 %. The ^{1}H NMR spectrum (400 MHz, $CDCl_3$) displayed δ values at 8.07 (d, J = 6.9 Hz, 2H), 7.44 (s, 4H), 7.22 (s, 2H), 5.76–5.45 (m, 4H), 4.50 (d, J = 42.5 Hz, 4H), 3.66 (s, 2H), 3.33–3.23 (m, 4H), 2.98–2.47 (m, 8H), 2.13–2.04 (m, 2H), 1.74–1.57 (m, 4H), 1.25 (q, J = 6.7 Hz, 9H), 0.87 (t, J = 6.6 Hz, 6H).

(c) Poly(Et-Hex/Ph – NDI) copolymer 3 (P3)

Following the established copolymerization methodology, phenyl-substituted-NDI (Ph-NDI) was employed as the comonomer. The reaction afforded (155 mg) of product as an off-white crystalline material, representing an isolated yield of 78 %. The ^{1}H NMR spectrum (400 MHz, $CDCl_3$) displayed δ values at 7.46–7.20 (m, 6H), 5.82–5.49 (m, 4H), 3.32–2.67 (m, 10*H*), 2.17 (d, J = 27.9 Hz, 2H), 1.71 (d, J = 4.6 Hz, 4H), 1.25–1.22 (m, 9H), 0.87 (t, J = 6.4 Hz, 6H).

(d) Poly(Et-Hex/F_5Ph – NDI) copolymer 4 (P4)

Following the established copolymerization methodology, pentafluorophenyl-substituted-NDI (F_5Ph-NDI) was employed as the comonomer. The reaction afforded (166 mg) of product as an off-white crystalline material, representing an isolated yield of 83 %. The ^{1}H NMR spectrum (400 MHz, $CDCl_3$) displayed δ values at 5.76–5.50 (m, 4H), 3.32–2.66 (m, 10*H*), 2.24–2.06 (m, 2H), 1.71–1.53 (m, 4H), 1.24 (q, J = 6.9 Hz, 9H), 0.86 (t, J = 6.6 Hz, 6H).

(e) Poly(Et-Hex/Adm – NDI) copolymer 5 (P5)

Following the established copolymerization methodology, adamantyl-substituted-NDI (Adm-NDI) was employed as the comonomer. The reaction afforded (138 mg) of product as an off-white crystalline material, representing an isolated yield of 69 %. The ^{1}H NMR spectrum (400 MHz, $CDCl_3$) displayed δ values at 5.76–5.45 (m, 4H), 3.34–2.64 (m, 10*H*), 2.37 (s, 6H), 2.09 (s, 5H), 1.73–1.55 (m, 10*H*), 1.24 (t, J = 6.6 Hz, 9H), 0.88–0.85 (m, 6H).

(f) Poly(Et-Hex/Cy-Hex – NDI) copolymer 6 (P6)

Following the established copolymerization methodology, cyclohexyl-substituted-NDI (Cy-Hex-NDI) was employed as the comonomer. The reaction afforded (133 mg) of product as an off-white crystalline material, representing an isolated yield of 67 %. The ^{1}H NMR spectrum (400 MHz, $CDCl_3$) displayed δ values at 5.74–5.50 (m, 4H), 3.90–3.84 (m, 1H), 3.34–2.64 (m, 10*H*), 2.12–2.06 (m, 4H), 1.80–1.53 (m, 8H), 1.25–1.16 (m, 11*H*), 0.88–0.85 (m, 6H).

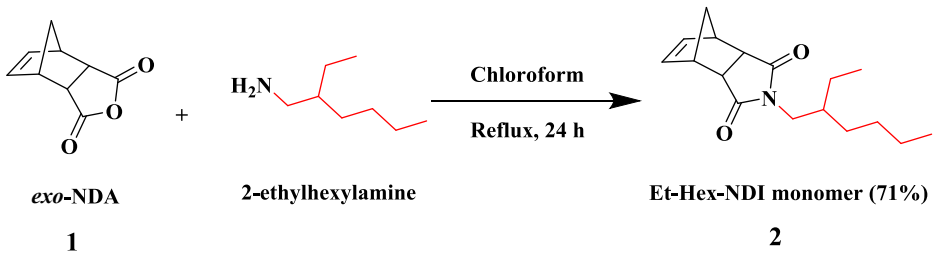

Scheme 1. Preparation Pathway of (Et-Hex-NDI) monomer.

3. Results and discussion section

3.1. Design and characterization of (Et-Hex-NDI) monomer

As illustrated in Scheme 1, the Et-Hex-NDI monomer was synthesized through the imidization of *exo*-NDA. In a representative procedure, *exo*-NDA was treated with 2-ethylhexylamine in chloroform under reflux conditions. Subsequent purification afforded the target monomer as a colorless oil in 71 % yield. The structural characterization of the Et-Hex-NDI monomer is supported by the mass and NMR spectra presented in Fig. S2 (**A**-**E**). The EI-MS spectrum (Fig. S2**A**) confirms the molecular identity, showing a dominant molecular ion peak at 275.00. The ^{1}H NMR spectrum (Fig. 1) displays key resonances of the norbornene moiety, a characteristic triplet at 6.26 ppm ($J = 1.8$ Hz) for the olefinic proton (a), a triplet at 3.25 ppm ($J = 1.6$ Hz) and a doublet at 2.65 ppm ($J = 1.3$ Hz) for the bridgehead protons (b and d). The ethylhexyl side chain is evidenced by a multiplet at 3.37–3.31 ppm for the *N*-adjacent methylene protons (e), a complex multiplet near 1.50 ppm for the internal methylenes, and a terminal two methyl multiplet at 0.87–0.84 ppm. The ^{13}C NMR spectrum (Fig. S2**B**) shows carbonyl carbons at 178.48 and 178.49 ppm (C-5), the olefinic carbon at 137.89 ppm (C-1), and aliphatic carbon atoms between 10.41 and 47.84 ppm. Two-dimensional NMR analyses further validate the structure. The COSY spectrum (Fig. S2**C**) confirmed proton connectivity through scalar couplings, revealing distinct cross-peaks for vicinal pairs (a-2H/b-2H, e-2H/f-1H, h-3H & l-3H/g-2H & k-2H, j-2H/k-2H). The DEPT spectrum (Fig. S2**D**) differentiated carbon types, with positive signals for CH/CH_3 groups (e.g., 137.89, 47.84, 45.23, 37.81, 14.11, 10.41 ppm) and negative signals for CH_2 groups (e.g., 42.85, 42.61, 30.58, 28.48, 23.98, 23.04 ppm), while the carbonyl carbons (178.48, 178.49 ppm) were absent as expected. Finally, the HMQC spectrum (Fig. S2**E**) provided direct ^{1}H–^{13}C one-bond correlations, unambiguously assigning all protons (a-l) to their respective carbon resonances.

3.2. Monitoring of poly(Et-Hex–NDI) homopolymerization

Scheme 2 presents the homopolymerization of Et-Hex–NDI monomer and the corresponding kinetic study. The reaction was performed using G1 catalyst targeting a degree of polymerization of ~ 50 units. This targeted molecular weight range was chosen to optimize polymerization efficiency by reducing chain termination occurrences and decreasing solution viscosity [61]. Polymerization was quenched at various times (1–90 min) with excess EVE. ^{1}H NMR analysis of unquenched samples showed a steady decrease in olefinic proton signals (*) alongside

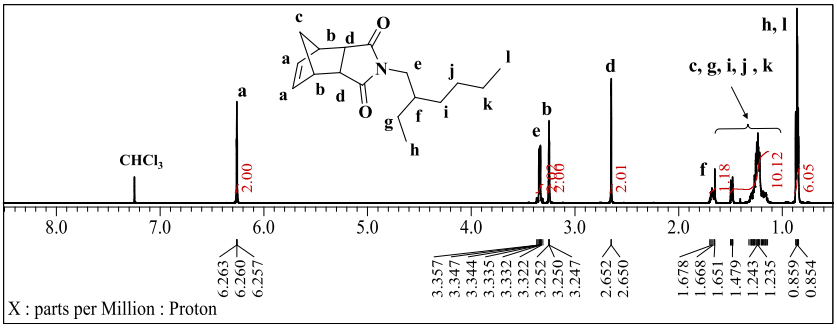

Fig. 1. ^{1}H NMR Spectrum of Et-Hex-NDI monomer.

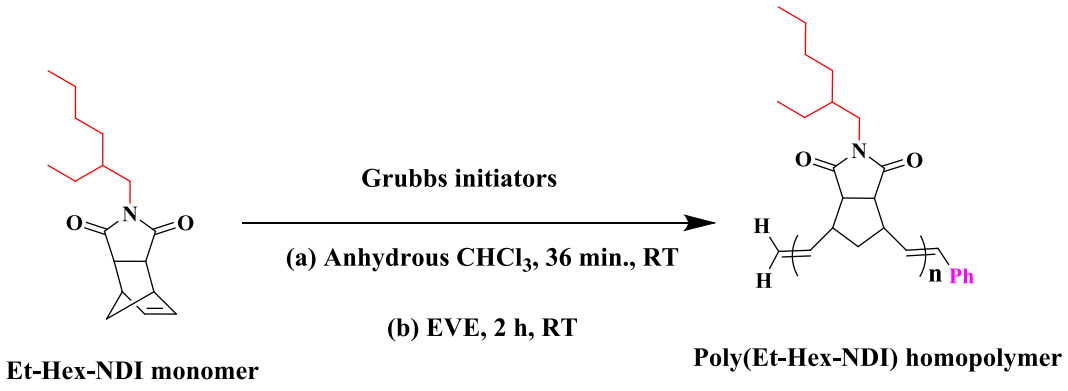

Scheme 2. Synthetic approaches to the poly (Et-Hex-NDI) homopolymer.

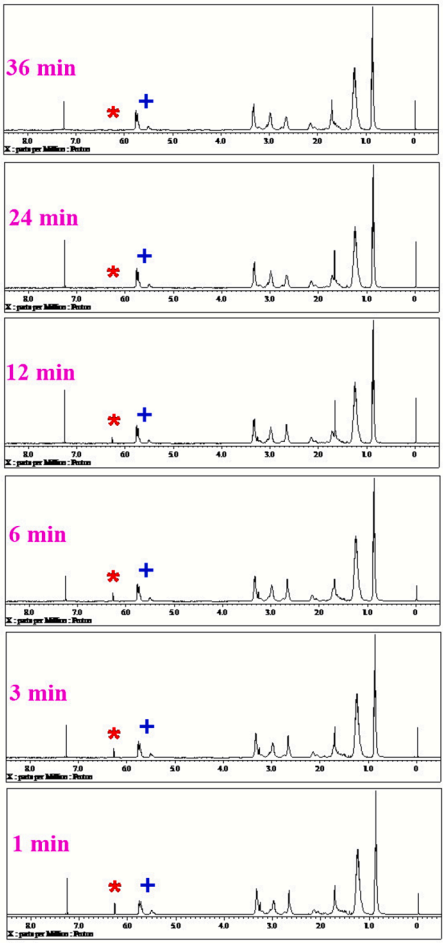

Fig. 2. The ^{1}H NMR spectra of monomer conversion from 1 to 36 min; (*) and (+) denote monomer and polymer peaks, respectively.

increasing cis- and *trans*-vinylene (+) polymer peaks, indicating monomer conversion. Complete consumption of the monomer was achieved by nearly 36 min (Fig. 2). Also, **Fig. S5** provides NMR monitoring over 48–90 min, confirming monomer depletion and concurrent polymer chain growth, while also resolving the formation of cis and trans stereoisomers via their distinct chemical shifts. As illustrated **in** Fig. 3, the ^{1}H NMR spectrum of poly(Et-Hex-NDI) verified the polymer structure. Key vinylene resonances for trans and cis isomers were observed at 5.76 and 5.49 ppm, respectively. Methylene (e) and methine (b, d, f) protons appeared as characteristic multiplets and a doublet (J = 41.2 Hz). Aliphatic methylene and methine signals (c, g, i, j, k) resonated between 1.21–1.73 ppm, with terminal methyl groups (h, l) at 0.85–0.89 ppm. GPC results (Fig. 4**(A-C)**, Table 1) reveal that the molecular weights of poly(Et-Hex–NDI), including M_n, M_w, and M_p, rise rapidly during the first 1–36 min of polymerization, after which the values stabilize, indicating that the polymerization reaches completion. The M_w shows a continuous shift toward higher molecular weights on the Log M scale during this initial phase. Throughout the reaction, the PDI remains nearly constant, demonstrating that the polymer growth occurs in a controlled manner with minimal widening of the molecular weight distribution.

3.3. *Living character via [Monomer/Initiator] ratio study*

A series of homopolymers with targeted degrees of polymerization (50–300) were synthesized to assess living behavior. Consistent with prior studies, polymerization using the Grubbs (G1) initiator afforded a polymer backbone with a predominant *trans*-vinylene configuration (84:16 trans/cis), a consequence of the specific G1 ligand environment [59]. Fig. 5 (**A**–**C**) and Table 2 summarize the polymerization behavior of poly(Et-Hex-NDI) homopolymer, revealing systematic variation in molecular weight with the monomer-to-initiator ratio. Both M_n and M_w increase linearly as the initiator concentration decreases, consistent with a well-regulated, living ROMP process. The GPC traces show uniform shifts along the Log M axis with narrow dispersities (PDI < 1.3), confirming controlled growth and minimal termination or transfer events. Although the experimentally observed M_n values exceed theoretical predictions, their linear dependence on the targeted degree of polymerization further supports a living mechanism. Slight PDI broadening at the highest polymerization degree (n = 300) indicates minor loss of control at extended chain lengths, a common feature in such systems [62].

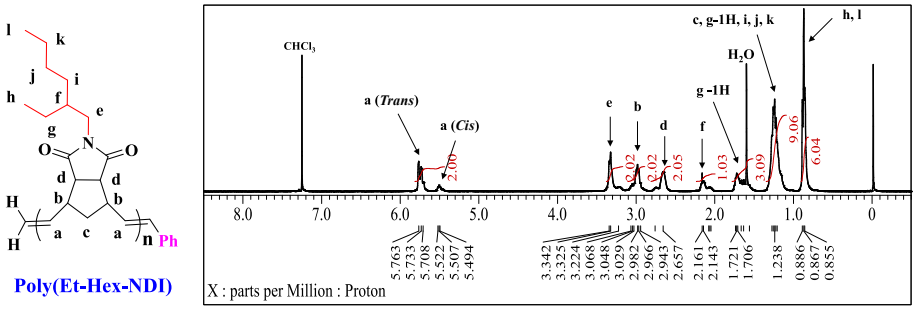

Fig. 3. The ^{1}H NMR spectrum of poly(Et-Hex-NDI) homopolymer.

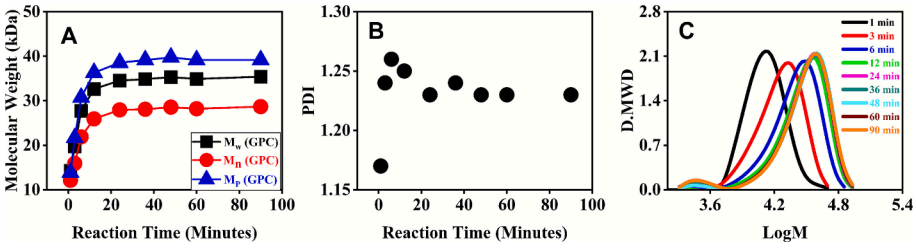

Fig. 4. (**A**) GPC-measured molecular weight versus reaction time, (**B**) PDI changes during the reaction, and (**C**) GPC traces at different time intervals.

Table 1
GPC data regarding the tracking of the homopolymerization reaction.

Reaction Time (Minutes) [a]	M_n [c] [GPC] (kDa)	M_w [b] [GPC] (kDa)	M_p [d] [GPC] (kDa)	PDI [e]
1	12.14	14.27	13.85	1.17
3	15.91	19.75	21.65	1.24
6	21.89	27.72	30.72	1.26
12	25.94	32.66	36.29	1.25
24	27.93	34.51	38.54	1.23
36	28.09	34.86	39.13	1.24
48	28.55	35.30	39.72	1.23
60	28.21	34.91	39.13	1.23
90	28.67	35.40	39.13	1.23

[a] The monomer-to-initiator ratio was calculated as n = 50 for all polymerizations at different time points using the G1 catalyst.
[b] M_w represents the weight-average molecular weight.
[c] M_n denotes the number-average molecular weight.
[d] M_p corresponds to the peak molecular weight.
[e] PDI refers to the polydispersity index.

3.4. Effect of Grubbs initiators on homopolymerization

To better understand the living nature of ROMP and compare the effectiveness of different Grubbs initiators on Et-Hex-NDI monomers, polymerization reactions were conducted using HG1, HG2, G3, and G2 initiators. These reactions were carried out at ambient temperature, aiming for a targeted degree of polymerization of 50 over 36 min. Termination was achieved by the addition of EVE, followed by polymer isolation through precipitation in excess methanol. The resulting homopolymers exhibited ^{1}H NMR spectra, comparable to those prepared with the G1 catalyst. Nonetheless, notable differences in the olefinic proton signals suggested variations in *cis/trans* isomer distributions, which were dependent on the catalyst employed. Integration of ^{1}H NMR peaks indicated that G1 and HG1 predominantly favored the formation of *trans* double bonds (83–84 %), whereas HG2, G3, and G2 yielded polymers with a significantly higher *cis* content (46 %), a trend attributed to their bulkier ligand environments and accelerated initiation and propagation kinetics. GPC data (Table 3 and Fig. 6) demonstrated that G1 facilitated the most controlled polymerization, yielding polymers with relatively narrow molecular weight distributions (PDI = 1.21) and an average molecular weight (M_n) of 31.14 kDa. In comparison, polymers synthesized with HG1, HG2, G3, and G2 showed broader dispersities (PDI ranging from 1.39 to 1.69). These results collectively suggest that G1 remains the most effective catalyst for polymerizing highly strained norbornene monomers under the conditions studied.

3.5. Characterization of copolymers (P1-P6)

Scheme 3 details the synthesis of random copolymers of Et-Hex-NDI with various norbornene dicarboximide comonomers (PT-NDI, Cbz-NDI, Ph-NDI, F5Ph-NDI, Adm-NDI, Cy-Hex-NDI). Guided by the homopolymerization kinetics, all copolymerizations were conducted with catalyst **G1** and targeted for a degree of polymerization of 50 to optimize processability. This standardized protocol employing equimolar

Table 2
GPC Analysis of Et-Hex-NDI Living Homopolymerization.

n [a]	M_n [Cal.] [b] (kDa)	M_n [GPC] [c] (kDa)	M_w [GPC] (kDa)	PDI	Yield %	*Cis*: *Trans* Content [d]
50	13.75	31.14	37.88	1.21	61	17:83
100	27.50	68.20	80.90	1.18	72	16:84
150	41.25	106.85	125.26	1.17	83	17:83
200	55.00	119.71	144.55	1.20	73	16:84
250	68.75	167.52	218.33	1.30	77	17:83
300	82.50	178.49	340.21	1.90	52	16:84

[a] The monomer-to-initiator ratios.
[b] M_n is estimated based on the theoretical number of repeating units (n = 50 - 300).
[c] M_n observed from GPC analysis.
[d] the (*Cis*: *Trans*) content determined from NMR charts.

Table 3
Effect of Grubbs Catalyst on Living Homo-Polymerization of Et-Hex-NDI.

Grubbs catalyst [a]	M_n [GPC] (kDa)	M_w [GPC] (kDa)	PDI	Yield %	*Cis*: *Trans* Content [b]
G1	31.14	37.88	1.21	61	17:83
HG1	145.04	202.90	1.39	86	16:84
HG2	226.73	349.98	1.54	97	46:54
G3	285.47	458.23	1.60	79	46:54
G2	914.52	1550.62	1.69	89	46:54

[a] The [Monomer/initiator] ratio was set at (n = 50) for all polymerizations at different initiators.
[b] identified by ^{1}H NMR spectroscopy.

comonomer feeds and a 36-minute reaction time successfully afforded a series of copolymers in good to excellent yields (67–83 %), enabling a direct comparative analysis. The chemical structures of the poly(Et-Hex-NDI) homopolymer and its copolymers (P1–P6) were analyzed using FT-IR spectroscopy over the range of 500–4000 cm^{-1}, as shown in Fig. 7, to investigate their vibrational characteristics. All samples displayed characteristic absorption bands at 748–767 cm^{-1} and 968–989 cm^{-1}, corresponding to the *cis* and *trans* olefinic stretching modes, respectively. Peaks observed around 1395 cm^{-1} and 2950 cm^{-1} are assigned to the bending and stretching vibrations of methyl (–CH_3) groups, originating from the terminal methyl units of the ethylhexyl side chains. Vibrational bands observed around 1700 cm^{-1} and 1770 cm^{-1} are assigned to the symmetric and asymmetric (–CONH–) stretching modes of the norbornene imide core. In copolymers P1 and P2, the peaks around 1738 and 1739 cm^{-1} are indicative of ester carbonyl groups, originating from the side-chain ester functionalities of the comonomers, respectively. Additionally, absorptions in the 2856–2867 cm^{-1} and 2912–2932 cm^{-1} regions correspond to the symmetric and asymmetric (–CH_2–) stretching vibrations within the polymer backbone, respectively. All synthesized copolymers were characterized by ^{1}H NMR spectroscopy (Fig. 8). The ^{1}H NMR spectra exhibited characteristic broad polymer resonances, confirming the polymeric norbornene scaffold. Key vinylene proton signals appeared between 5.45 and 5.82 ppm,

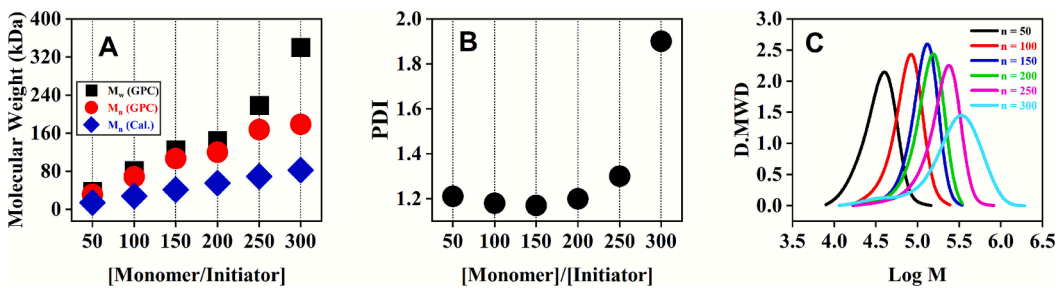

Fig. 5. (**A**) Molecular weights, (**B**) PDI values, and (**C**) GPC traces for various [Monomer/Initiator] ratios of poly(Et-Hex-NDI) homopolymer.

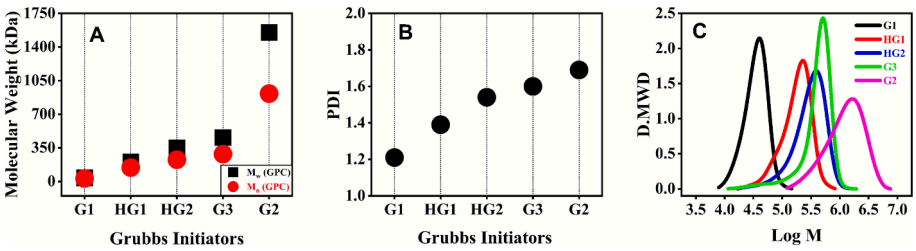

Fig. 6. (**A**) Molecular weights by GPC, (**B**) PDI values, and (**C**) GPC traces of the poly(Et-Hex-NDI) homopolymer of different Grubbs initiators.

while other multiplets were consistent with the bridged bicyclic structure of the backbone. Furthermore, definitive signals from the ethylhexyl side chain were consistently present, identified as a methylene multiplet at ~ 1.24 ppm and terminal methyl groups at ~ 0.87 ppm. The unique comonomer in each copolymer provided distinct NMR signatures. The aromatic protons of the phenothiazine unit in P1 (Fig. 8**A**) appeared as a quartet at 7.13 ppm and a doublet at 6.92 ppm. Similarly, the carbazole aromatics in P2 (Fig. 8**B**) were observed as broad signals between 8.07 and 7.22 ppm. For P3 (Fig. 8**C**), the phenyl group's aromatic protons appeared as a multiplet between 7.46 and 7.20 ppm. In contrast, the pentafluorophenyl spectrum of P4 Fig. 8**D**) showed no aromatic proton signals, with its successful incorporation instead confirmed by three distinct sets of fluorine signals in the ^{19}F-NMR spectrum, as shown in Fig. 8**E**. Copolymers with aliphatic side chains, P5 (adamantyl) and P6 (cyclohexyl), exhibited broad, complex signals in the 1.0–3.0 ppm region. For P5 Fig. 8**F**), singlets at 2.37 and 2.09 ppm were assigned to the adamantyl methylene and methine protons, respectively. For P6, a distinctive multiplet at 3.90–3.84 ppm was attributed to the cyclohexyl methine proton as presented in Fig. 8**G**. Collectively, the NMR data confirm the successful formation of all target copolymer structures via living ROMP.

Fig. 9 **(A and B)** depicts the molecular weight profiles of the obtained random copolymers, while Fig. 9**C** presents the corresponding GPC traces for systems incorporating different NDI-substituted units. The homopolymerization of poly(Et-Hex-NDI) (Mn = 31.14 kDa, PDI = 1.21) was previously completed within 36 min, achieving full monomer conversion and a targeted degree of polymerization of n = 50. To ensure comparability, subsequent copolymerizations were conducted under identical experimental parameters, with only the NDI-functionalized comonomer structures being varied. The M_n molecular weights for the copolymers were determined as follows: P1 = 59.23 kDa (PDI = 1.15), P2 = 65.89 kDa (PDI = 1.20), P3 = 43.41 kDa (PDI = 1.18), P4 = 56.16 kDa (PDI = 1.24), P5 = 52.61 kDa (PDI = 1.15), and P6 = 53.01 kDa (PDI = 1.18). In every case, the M_n exceeded that of the homopolymer, while PDIs remained narrow, approaching Poisson-type distributions, indicative of well-regulated copolymer growth and similar monomer reactivity ratios. All copolymers exhibited a predominance of *trans* configurations (80–89 %) over *cis* configurations (11–20 %), a

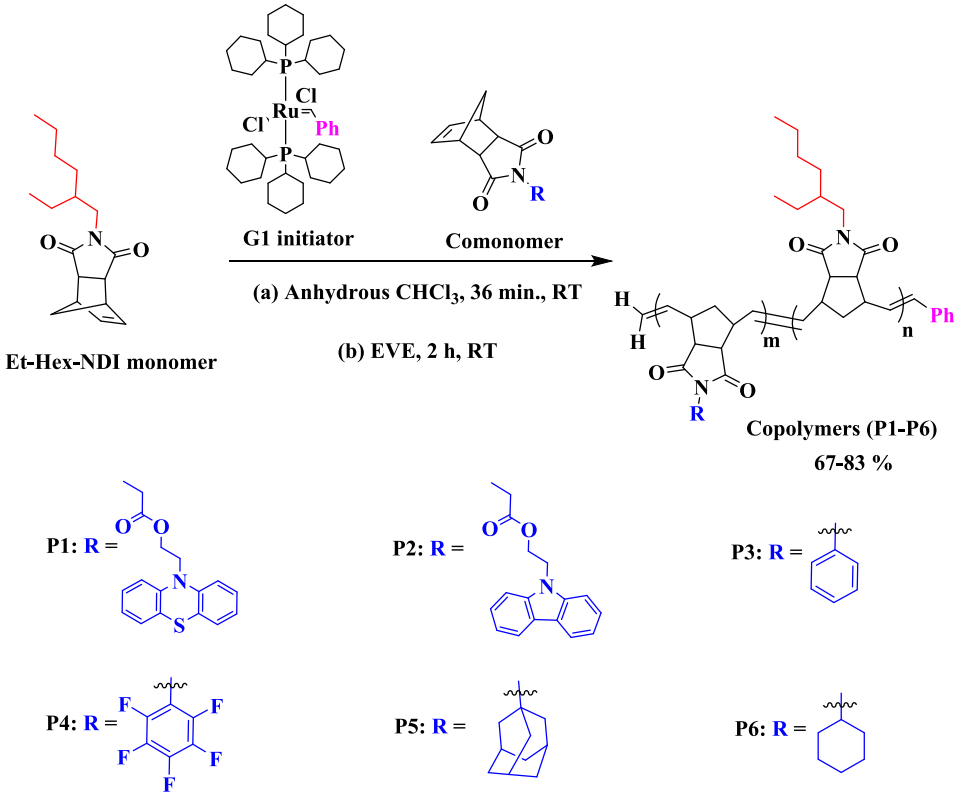

Scheme 3. The synthetic approaches of copolymers (P1-P6).

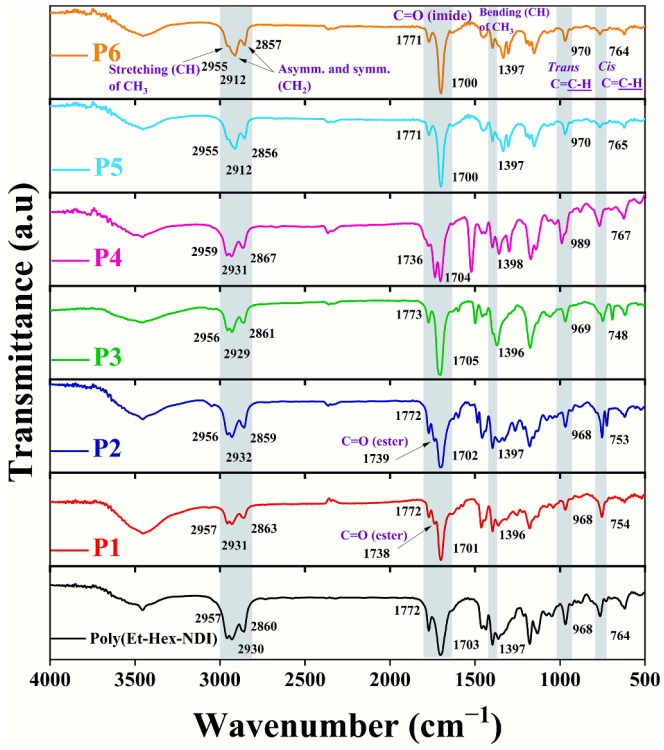

Fig. 7. FT-IR spectra of the poly(Et-Hex-NDI) homopolymer and its copolymers (P1–P6).

stereochemical outcome ascribed to the ligand environment of the G1 catalyst, which reduces steric congestion and results in a relatively slower initiation rate, as summarized in Table 4.

3.6. Side-chain impact on physical properties of the synthesized polymers

3.6.1. Optical properties

The optical properties of the poly(Et-Hex-NDI) homopolymer and its copolymers were investigated using UV–visible spectroscopy (200–900 nm) in dilute THF solution (10^{-6} M) at room temperature (Fig. 10, Table 5). The unsubstituted *exo*-NDA precursor exhibited a distinct absorption maximum at 228 nm, attributable to the n–π* transition of the carbonyl group. Upon ethylhexyl substitution and subsequent polymerization, poly(Et-Hex-NDI) displayed two absorption bands at approximately 231 nm and 252 nm. The band at 231 nm reflects the n–π* transition, whereas the 252 nm feature is ascribed to a new transition arising from the electron-donating influence of the ethylhexyl substituent. Incorporation of phenothiazine and carbazole units into the polymer backbone (P1 and P2, respectively) *via* copolymerization resulted in noticeable variations of the optical absorption profile. Both polymers exhibited a distinct hyperchromic effect, accompanied by the appearance of additional absorption bands at longer wavelengths compared to the parent poly(Et-Hex-NDI). Specifically, P1 displayed absorption bands at 256 and 313 nm, while P2 featured multiple bands at 260, 292, 327, and 342 nm. The most pronounced absorptions were observed at λ_{max} = 313 nm for P1 and λ_{max} = 342 nm for P2, corresponding to red-shifts of approximately 61 nm and 90 nm, respectively, relative to the parent homopolymer. The combination of significant bathochromic shifts with enhanced absorption intensity underscores the extension of π-conjugation imparted by the electron-rich phenothiazine and carbazole moieties, highlighting their role in modulating the electronic structure of the resulting copolymers. In contrast, copolymers P3–P6, which lack strongly conjugated donor substituents, exhibited distinctly different absorption features. Their spectra were restricted to shorter wavelengths, with primary bands observed within 251–261 nm. Furthermore, P3–P6 demonstrated a pronounced hypochromic effect, displaying reduced absorption intensity relative to poly(Et-Hex-NDI). This behavior can be attributed to the incorporation of less electron-rich groups, diminishing the absorption strength. The absorption onset values (λ_{onset}) for poly(Et-Hex-NDI) and copolymers P1–P6 were determined as 277, 349, 351, 278, 280, 279, and 274 nm, corresponding to optical bandgap energies (E_g^{op}) of 4.48, 3.55, 3.53, 4.46, 4.43, 4.44, and 4.53 eV, respectively. Relative to the *exo*-NDA precursor (λ_{max} = 228 nm), the poly(Et-Hex-NDI) homopolymer exhibited a red-shifted absorption maximum at 252 nm, reflecting a modest enhancement in optical absorption. The relatively wide bandgap range (3.53–4.53 eV) underscores the potential of these materials for optoelectronic applications that demand high transparency, including protective coatings, optically clear films, and encapsulation layers [63,64]. Furthermore, the observed absorption maxima extend beyond those of sulfonated NDI-based derivatives, which typically absorb at significantly shorter wavelengths (196–200 nm), as reported in prior literature [65].

3.6.2. Thermal behavior

The thermal stability of the polymers, governed by backbone rigidity and side-group structures, is critical for their practical utility. To evaluate these properties, TGA, DTG, and DSC measurements were carried out under argon. Polymers bearing ethylhexyl groups exhibit unexpectedly high thermal stability in both homopolymer and copolymer forms. Contrary to the typical plasticizing role of ethylhexyl chains, the rigid norbornene-imide backbone counteracts this effect within a single macromolecular architecture. As depicted in Fig. 11**A**, poly(Et-Hex-NDI) exhibits a one-step degradation at 454 °C with 84.5 % mass loss, assigned to main-chain scission. The high T_d arises from the rigid bicyclic norbornene core, resonance-stabilized imide units, and steric shielding by ethylhexyl groups, which collectively suppress radical-mediated degradation. Furthermore, Fig. 11**B** depicts the DSC thermogram of the homopolymer, exhibiting a glass transition at 168 °C. While ethylhexyl substituents are generally linked with lower T_g values due to their plasticizing effect, the observed T_g remains high. This is explained by the rigid norbornene bicyclic framework, which restricts chain motion, and the resonance-stabilized dicarboximide unit, which further limits segmental mobility. In addition, the covalently bound bulky ethylhexyl side groups introduce steric hindrance that limits rotational relaxation, while the absence of flexible spacers promotes tighter molecular packing, collectively preserving the elevated T_g [66].

Copolymerization of Et-Hex-NDI with different comonomers afforded copolymers (P1–P6) exhibiting high thermal stability, with decomposition temperatures (T_d) ranging from 358 to 459 °C and initial weight losses of 27.2–88.5 % (Fig. 12 **(A-F)**, Table 6). The Tds for P1–P6 were 393, 358, 451, 444, 456, and 459 °C, respectively. Among them, only P1 and P2 displayed two-step degradation behavior. The first weight-loss stage occurred at 393 °C (P1, 35 %) and 358 °C (P2, 27.2 %), which can be attributed to the smaller fraction of phenothiazine or carbazole side chains incorporated into their backbones. These heteroaromatic moieties are less thermally stable than ethylhexyl-substituted NDI, as the heteroatoms and conjugated rings of phenothiazine and carbazole are more susceptible to oxidation or bond cleavage at lower temperatures. Consequently, ester-linked heteroaromatic units degrade earlier than the more stable ethylhexyl-NDI segments. The second

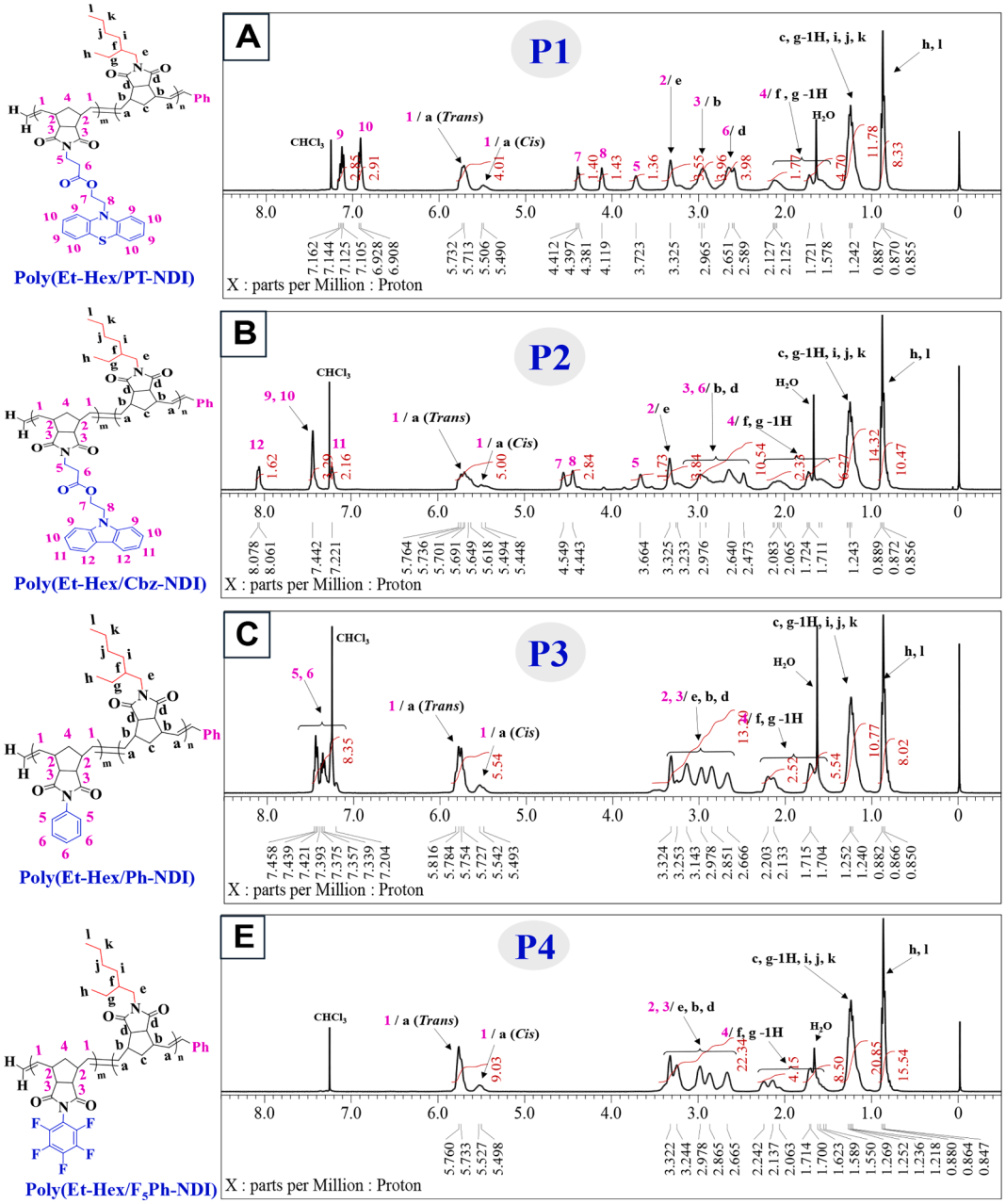

Fig. 8. The NMR spectra of the copolymers: (**A**) ^{1}H NMR of P1, (**B**) ^{1}H NMR of P2, (**C**) ^{1}H NMR of P3, (**D**) ^{1}H NMR of P4, € ^{19}F NMR of P4, (**F**) ^{1}H NMR of P5, and (**G**) ^{1}H NMR of P6.

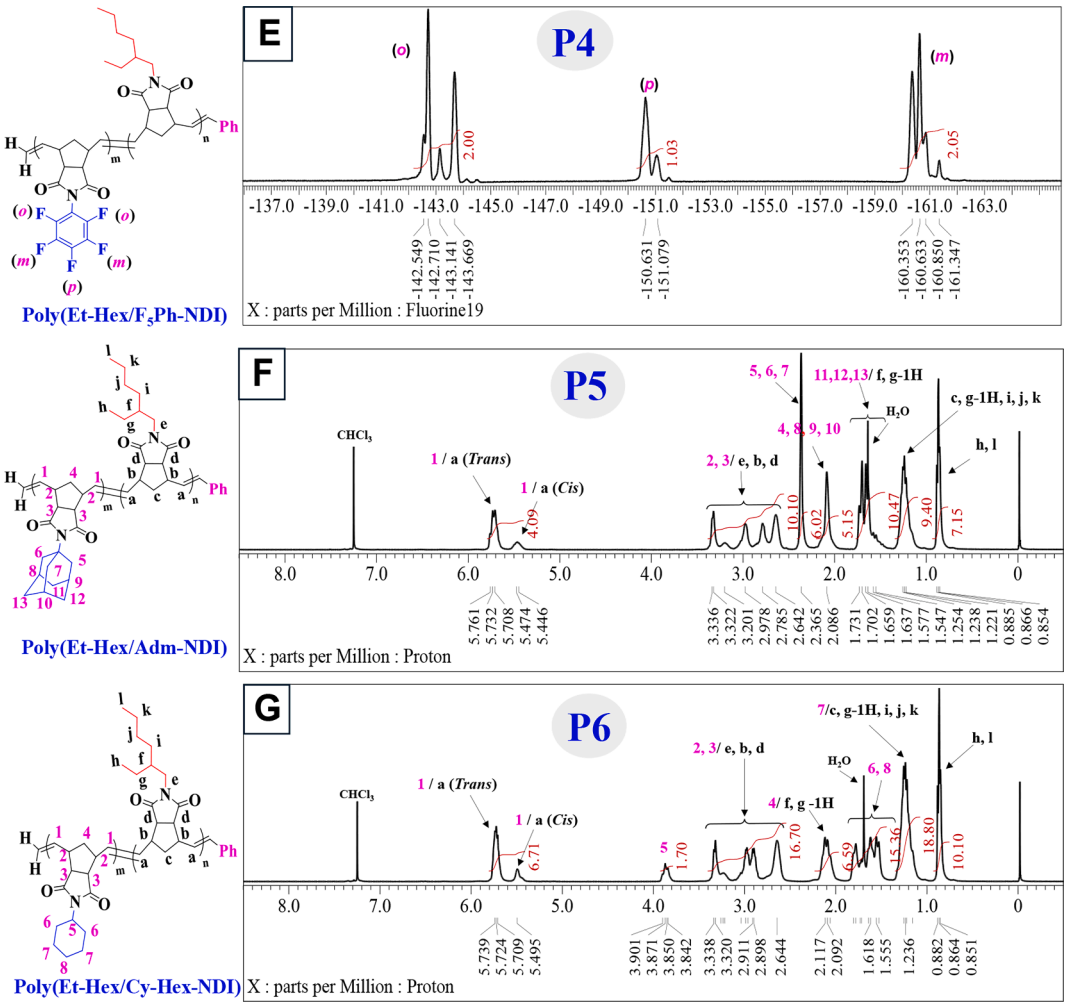

Fig. 8. (*continued*).

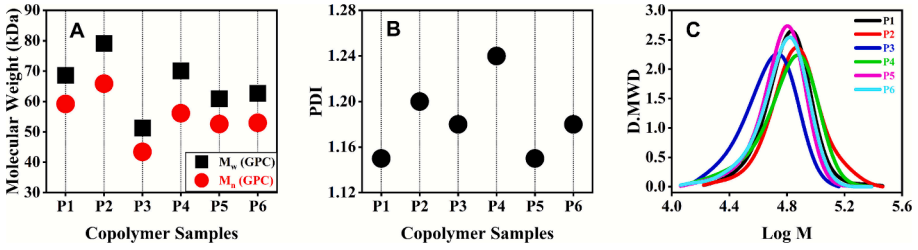

Fig. 9. (**A**) GPC-based molecular weights, (**B**) copolymer PDIs, and (**C**) corresponding chromatograms.

decomposition step for P1 and P2 occurred at 447 °C and 446 °C, with higher weight losses (46.4 % and 58.4 %), corresponding to the breakdown of the main NDI-based backbone. In contrast, copolymers P3–P6, incorporating phenyl, pentafluorophenyl, adamantyl, and cyclohexyl side chains directly attached to the norbornene core, exhibited a single decomposition event at 451, 444, 456, and 459 °C, respectively, with major weight losses (72.7–88.5 %). This single-step behavior arises from the absence of easily cleavable ester linkages. Their high Tds, comparable to that of the homopolymer, indicate that both aromatic and aliphatic substituents effectively enhance polymer stability. Above 459 °C, progressive degradation continued, leaving 11.5–27.3 % char residue at 700 °C. Overall, the synthesized homo- and copolymers exhibited significantly higher T_ds than previously reported norbornene-based systems. While comparable NDI polymers containing tricarbazole, phenyl, cyclohexyl, or adamantyl substituents decomposed at 385–424 °C, and phosphonated or brush-type analogs degraded at 300–330 °C [42,49,67–69]. This enhanced robustness is attributed to the synergistic stabilization imparted by ethylhexyl groups integrated within the norbornene-NDI backbone.

DSC analysis was conducted to determine the glass transition temperature (T_g), which influences polymer flexibility and mechanical stability. Copolymerization of Et-Hex-NDI with various NDI derivatives resulted in significant T_g variations, generally lower than the homopolymer (168 °C). The T_g values for copolymers P1–P6 were 86, 102, 158, 143, 155, and 145 °C, respectively, as shown in Fig. 13 **(A-F)** and Table 6. The ethylhexyl-substituted homopolymer exhibits a high T_g (168 °C) due to steric hindrance and dense packing within the rigid norbornene core. In contrast, introducing phenothiazine- or carbazole-bearing comonomers significantly lowers T_g (86 and 102 °C, respectively), as these bulky aromatics are connected via flexible four-

Table 4
GPC data for copolymer samples (P1-P6).

Copolymer Samples	Copolymer (A: B) Composition [a] (%)	M_n [GPC] (kDa)	M_w [GPC] (kDa)	PDI	Yield %	*Cis*: *Trans* Content [b]
P1	66:34	59.23	68.67	1.15	75	16:84
P2	68:32	65.89	79.13	1.20	69	20:80
P3	51:49	43.41	51.30	1.18	78	14:86
P4	60:40	56.16	70.10	1.24	83	11:89
P5	54:46	52.61	60.90	1.15	69	14:86
P6	50:50	53.01	62.71	1.18	67	17:83

[a] Copolymer composition (A: B) determined from ^{1}H NMR spectra; A = mol fraction of Et-Hex-NDI monomer, while B = mol fraction (%) of the comonomer.
[b] the (*Cis: Trans*) content was determined using the ^{1}H NMR spectrum for each copolymer sample.

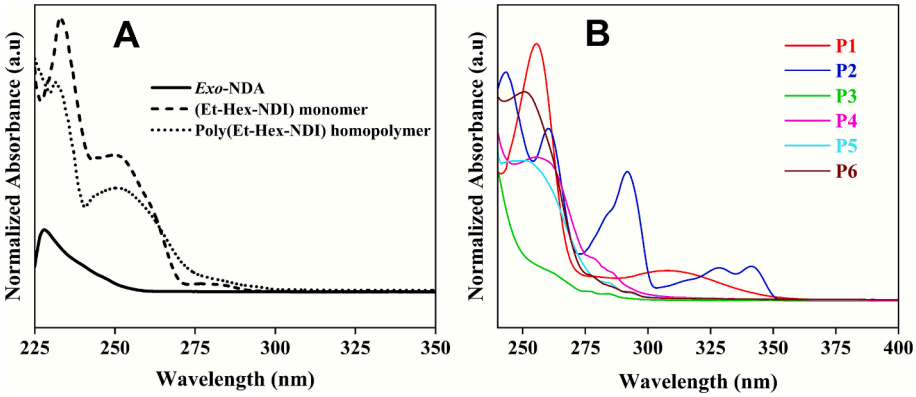

Fig. 10. UV - visible spectra:(**A**) for the poly(Et-Hex-NDI) and its synthetic precursors and (**B**) for the copolymers P1 - P6.

methylene ester spacers. These spacers act as compliant linkers that relieve steric strain, enabling pendant motion and promoting segmental relaxation at lower temperatures [70]. On the other hand, copolymers containing phenyl (158 °C), pentafluorophenyl (143 °C), adamantyl (155 °C), and cyclohexyl (145 °C) substituents display only moderate T_g reductions, reflecting the influence of side chains directly attached to the rigid norbornene framework. The adamantyl group limits chain motion but enlarges free volume; the phenyl ring enhances rigidity via π–π interactions; pentafluorophenyl substituents increase steric and electronic repulsion, disrupting packing; and the flexible cyclohexyl ring contributes moderate steric and free-volume effects, yielding an intermediate T_g decrease. DSC analysis reveals that side-chain structure and attachment mode critically affect T_g. Copolymers (P3–P6) with side chains directly bonded to the norbornene core show T_g values close to the parent homopolymer, while those with long spacers (P1, P2) exhibit markedly reduced T_g due to enhanced chain mobility and decreased packing. The high T_g of spacer-free homopolymers underscores the influence of spacer length and polymer architecture on thermal properties [71]. Except for P1 and P2, all copolymers exhibited remarkably high T_g values, surpassing previously reported systems such as NDI-cyclohexyl (129 °C) and indole-based polyesters (55–99 °C) [72,73]. Additionally, the homo- and copolymers showed distinct endothermic peaks at 256–258 °C, reflecting melting transitions associated with well-ordered crystalline domains in the polymer backbone.

Table 5
The Optical Properties of the Et-Hex-NDI Homo and Copolymers.

Samples	λ_{abs} (nm)	λ_{onset} (nm)	E_g^{op} (eV)[b]
Poly(Et-Hex-NDI)	252	277	4.48
P1	256, 313	349	3.55
P2	260, 292, 327, 342	351	3.53
P3	261	278	4.46
P4	258	280	4.43
P5	253	279	4.44
P6	251	274	4.53

[a]Polymer samples were determined in THF solution.
[b] The optical bandgap was calculated using the absorption onset from solution phase UV–visible spectroscopy, employing the relationship ($E_g^{op} = 1240/\lambda_{onset}$).

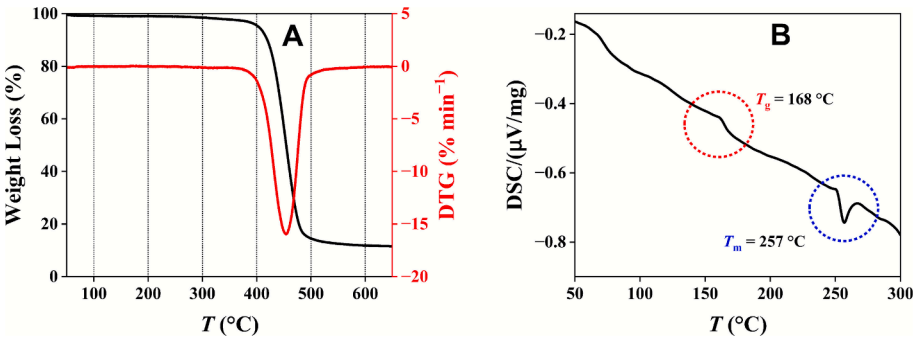

Fig. 11. (**A**) TGA and (**B**) DSC profiles of the poly(Et-Hex-NDI) homopolymer.

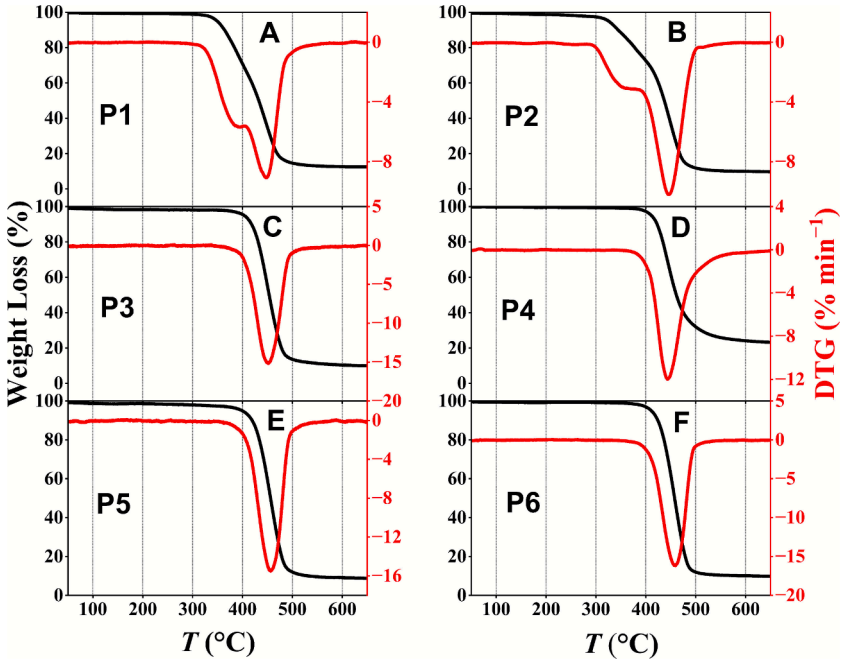

Fig. 12. TGA and DTG profiles of the copolymers: (**A**) P1, (**B**) P2, (**C**) P3, (**D**) P4, (**E**) P5, and (**F**) P6.

Table 6
Thermal properties of the synthesized homo and copolymers.

Samples [a]	W_t Loss [b] (%)	T_d [c] (°C)	Total wt Loss (%)	Residual (%)	T_g (°C)	T_m (°C)
Poly (Et-Hex-NDI)	84.5	454	84.5	15.5	168	257
P1	35, 46.4	393, 447	81.4	18.6	86	257
P2	27.2, 58.4	358, 446	85.6	14.4	102	257
P3	86.3	451	86.3	13.7	158	256
P4	72.7	444	72.7	27.3	143	257
P5	88.5	456	88.5	11.5	155	256
P6	87.4	459	87.4	12.6	145	258

[a] T_ds values were determined from DTG curves.
[b] In copolymers P1 and P2, two distinct T_ds are observed.
[c] For P1 and P2, two weight loss values are identified, each corresponding to the respective T_d.

3.6.3. *Morphological properties*

Thin films of the synthesized copolymers were prepared, and the detailed procedures for film preparation are provided in the Supporting Information (Section 2.2). Fig. 14 **(A-G)** presents FESEM micrographs illustrating the surface morphologies of the poly(Et-Hex-NDI) homopolymer and its copolymers (P1–P6), obtained through ROMP of ethylhexyl-substituted norbornene dicarboximide. Clear differences in surface features are evident among the samples, underscoring the impact of side-chain variations on polymer microstructure. These morphological divergences across P1–P6 underscore the significant impact of comonomer choice on phase characteristics and structural organization. A densely packed and relatively smooth morphology is observed for the homopolymer poly(Et-Hex-NDI), which aligns with its high glass transition temperature (T_g = 168 °C) arising from the rigid backbone and restricted segmental mobility. P1 displays a loosely packed, irregular morphology with open domains, which corresponds to enhanced chain mobility and is consistent with its lower T_g (86 °C) arising from the phenothiazine side groups. In contrast, P2 exhibits a moderately rough and less compact surface, aligning with its intermediate thermal stability and the observed T_g of 102 °C, attributed to the carbazole substituents. Among P3–P6, T_g values remain relatively high (143–158 °C), accompanied by more ordered morphologies. P3, containing simple phenyl side groups, presents a smooth and compact surface. P4, functionalized with pentafluorophenyl moieties, shows a finely textured, slightly granular morphology, reflecting the electronic effects of fluorinated substituents. P5, with sterically bulky adamantyl groups, exhibits a robust, tightly packed surface with well-defined domain boundaries. P6, bearing cyclohexyl units, demonstrates a moderately compact surface with slight roughness, representing an intermediate structural state. Overall, the compactness and density of P3–P6 morphologies are mirrored in their high T_g values, nearly matching the homopolymer, highlighting the strong correspondence between polymer structure and thermal transitions. Also, Fig. S6 showed the FESEM micrographs of homo and copolymers at higher magnification.

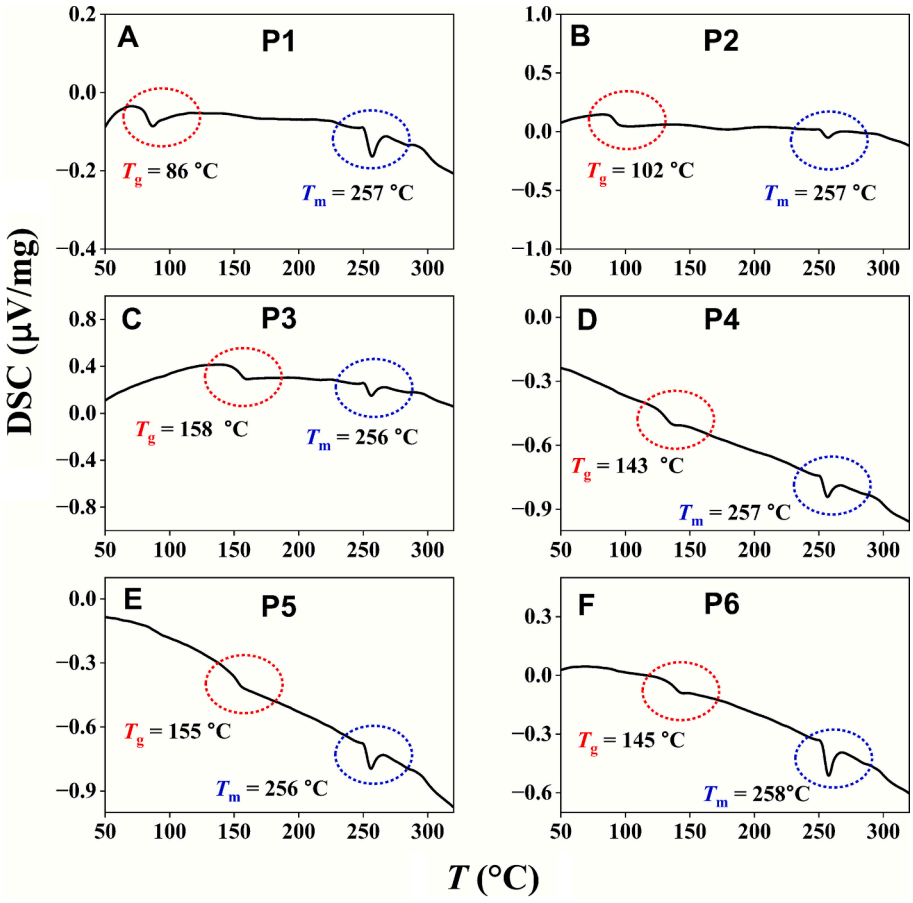

Fig. 13. DSC thermograms of the copolymers: (**A**) P1, (**B**) P2, (**C**) P3, (**D**) P4, (**E**) P5, and (**F**) P6.

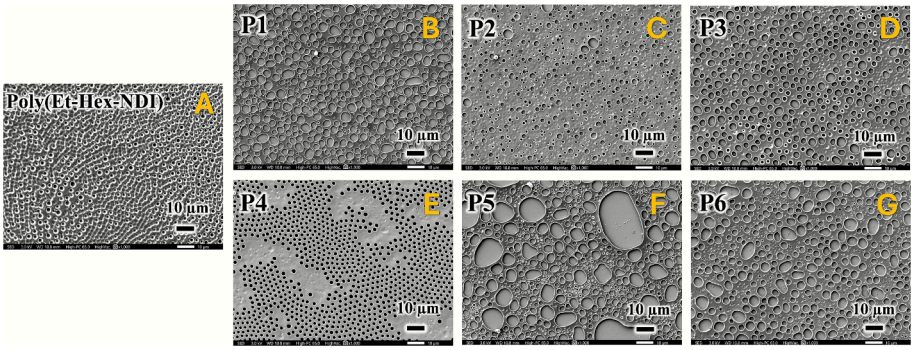

Fig. 14. ESEM micrographs of poly(Et-Hex-NDI) homopolymer (**A**) and its copolymers: (**B**) P1, (**C**) P2, (**D**) P3, (**E**) P4, (**F**) P5, and (**G**) P6.

4. Conclusion

This study provides a fundamental framework for the molecular engineering of norbornene dicarboximide polymers with tailored properties. We establish that the synergistic copolymerization of rigid norbornene cores with flexible ethylhexyl units is key to achieving the crucial balance between thermal stability and solution processability. The efficacy of G1 catalysis in producing well-defined polymers *via* a living ROMP mechanism was unequivocally confirmed, enabling precise synthetic control. Most significantly, we have decoded how side-chain functionality, specifically its steric bulk and electronic character, directly commands both the thermal and optoelectronic landscape of the resulting material. This ability to predictably manipulate properties through monomer design positions the Et-Hex-NDI platform as a highly versatile and rational starting point for developing next-generation functional polymers across diverse application domains.

CRediT authorship contribution statement

Mohammed F. Radwan: Writing – review & editing, Writing – original draft, Visualization, Validation, Software, Resources, Methodology, Investigation, Formal analysis, Data curation, Conceptualization. **Mohamed E. Abdu:** Reviewing – original draft, Visualization, Software. **Mahmoud Z. Basyouni:** Reviewing – review & editing, Visualization, Software. **Mostafa M. Elkady:** Writing – review & editing, Visualization, Software, Formal analysis. **Hiroshi Furuno:** Writing – review & editing, Project administration, Investigation, Funding acquisition. **Andrew M. Spring:** Writing – review & editing, Validation, Supervision, Project administration, Investigation, Funding acquisition, Data curation, Conceptualization.

Declaration of competing interest

The authors declare that they have no known competing financial interests or personal relationships that could have appeared to influence the work reported in this paper.

Acknowledgements

We gratefully acknowledge Professor Michitaka Ohtaki and Associate Professor Koichiro Suekuni, Interdisciplinary Graduate School of Engineering Sciences, Kyushu University, for their support with concrete thermal analysis measurements.

Appendix A. Supplementary material

Supplementary data to this article can be found online at https://doi.org/10.1016/j.eurpolymj.2025.114413.

Data availability

Data will be made available on request.

References

[1] J.A. Paquette, S. Ezugwu, V. Yadav, G. Fanchini, J.B. Gilroy, Synthesis, characterization, and thin-film properties of 6-oxoverdazyl polymers prepared by ring-opening metathesis polymerization, J. Polym. Sci., Part A: Polym. Chem. 54 (2016) 1803–1813, https://doi.org/10.1002/pola.28042.

[2] M.Z. Basyouni, M.E. Abdu, M.F. Radwan, A.M. Spring, From monomer to polymer: Controlled synthesis and comprehensive analysis of poly(p-phenylene vinylene) via ROMP, J. Mol. Struct. 1310 (2024) 138001, https://doi.org/10.1016/j.molstruc.2024.138001.

[3] M.E. Abdu, M.F. Radwan, D.A. Elsayed, W.S. Shehab, W.A. Zordok, M.Z. Basyouni, A.M. Spring, Controlled synthesis, characterization and computational studies of novel homo and random Co-polymers from carbazolovinylene and phenothiazinovinylene via ROMP chemistry, Polymer (Guildf). 333 (2025) 128590, https://doi.org/10.1016/j.polymer.2025.128590.

[4] M.Z. Basyouni, M.E. Abdu, M.F. Radwan, A.M. Spring, Ring-opening metathesis polymerization of homo- and copolymers based on p-phenylenevinylene and norbornene-dicarboximide: enhanced thermal stability for optoelectronic applications, J. Mol. Struct. 1338 (2025) 142296, https://doi.org/10.1016/j.molstruc.2025.142296.

[5] S. Rekha Rout, G. Kenguva, S. Mansuri, K.R. Manu, R. Dandela, N.B. Pramanik, Bottlebrush polymers via ring-opening metathesis polymerization (ROMP): Synthesis, properties and applications, Eur. Polym. J. 221 (2024) 113546, https://doi.org/10.1016/j.eurpolymj.2024.113546.

[6] J.C. Foster, J.T. Damron, H. Zhang, Simple monomers for precise polymer functionalization during ring-opening metathesis polymerization, Macromolecules 56 (2023) 7931–7938, https://doi.org/10.1021/acs.macromol.3c01068.

[7] A.F. Alahmadi, J. Zuo, F. Jäkle, B-N Lewis pair-fused dipyridylfluorene copolymers incorporating electron-deficient benzothiadiazole comonomers, Polym. J. 55 (2023) 433–442, https://doi.org/10.1038/s41428-022-00723-y.

[8] S.E. Blosch, S.J. Scannelli, M. Alaboalirat, J.B. Matson, Complex polymer architectures using ring-opening metathesis polymerization: synthesis, applications, and practical considerations, Macromolecules 55 (2022) 4200–4227, https://doi.org/10.1021/acs.macromol.2c00338.

[9] W. Hou, Y. Feng, Y. Zhou, X. Yin, H. Liu, Z. Liu, T. Zhao, Y. Shi, Y. Chen, Rapid and efficient synthesis of star polymers via arm-first monomer emulsified aqueous ring-opening metathesis polymerization (ME-ROMP), Macromolecules 57 (2024) 3173–3182, https://doi.org/10.1021/acs.macromol.4c00191.

[10] H. Wang, C. Ma, Z. Han, X. Liao, R. Sun, M. Xie, Efficient synthesis of trefoil-shaped tricyclic polymers by a ROMP-based blocking-cyclization technique, Polym. Chem. 15 (2024) 534–543, https://doi.org/10.1039/d3py01278f.

[11] M.F. Radwan, H.M. Dardeer, E.E. Elboray, M.F. Aly, Novel crystalline and thermally stable chitosan-chromone based polymers: Synthesis and characterization, J. Mol. Struct. 1241 (2021) 130625, https://doi.org/10.1016/j.molstruc.2021.130625.

[12] A.A. El-Shehawy, M.E. Abdu, M.M. El-Hendawy, M. El-Khouly, M.H. Sherif, H. Y. Moustafa, Synthesis, photophysical, and theoretical studies on π-conjugated copolymers based on benzothiadiazole and cyanopyridine acceptor moieties along with other π-bridge units, J. Phys. Org. Chem. 34 (2021) 1–15, https://doi.org/10.1002/poc.4158.

[13] F. Fan, C. Cai, L. Gao, J. Li, P. Zhang, G. Li, C. Li, G. Yu, Microwave-assisted synthesis of glycopolymers by ring-opening metathesis polymerization (ROMP) in an emulsion system, Polym. Chem. 8 (2017) 6709–6719, https://doi.org/10.1039/c7py01415e.

[14] B. Koo, D. Kim, D.Y. Song, W.J. Han, D. Kim, J.W. Park, M. Kim, C. Kim, The formation of photodegradable nitrophenylene polymers via ring-opening metathesis polymerization, Polym. Chem. 13 (2022) 6268–6273, https://doi.org/10.1039/d2py00684g.

[15] Y. Zuo, Y. Yao, C. Chen, Y. Liang, K.F. Yang, Z. Li, G.Q. Lai, P. Zhang, T.Y. Luh, Chemoselective ring-opening metathesis polymerization of cyclopropenes spirally appended with N-aryl saturated heterocycles, Polym. Chem. 14 (2022) 600–607, https://doi.org/10.1039/d2py01490d.

[16] P.V.R. Schleyer, J.E. Wiliiams, K.R. Blanchard, The evaluation of strain in hydrocarbons. The strain in adamantane and its origin, J. Am. Chem. Soc. 92 (1970) 2377–2386, https://doi.org/10.1021/ja00711a030.

[17] J. Asrar, Metathesis Polymerization of N-Phenylnorbornenedicarboximide, Macromolecules 25 (1992) 5150–5156, https://doi.org/10.1021/ma00046a006.

[18] M.E. Abdu, M.F. Radwan, A.E. Mesbah, Y.J. Hao, A. Zkria, M.Z. Basyouni, A. M. Spring, Living ROMP of poly(m,p-phenylenevinylene) and functionalized norbornene-dicarboximides copolymers: guided synthesis toward enhanced optoelectronic and thermal properties with DFT insights, Polym. Chem. 16 (2025) 4444–4469, https://doi.org/10.1039/D5PY00818B.

[19] M.J. Kim, Y.G. Yu, C.G. Chae, H. Bin Seo, J.S. Lee, Facile synthesis of amphiphilic bottlebrush block copolymers bearing pyridine pendants via click reaction from protected alkyne side groups, Macromolecules 53 (2020) 2209–2219, https://doi.org/10.1021/acs.macromol.9b02674.

[20] A.M. Spring, D. Maeda, M. Ozawa, K. Odoi, F. Qiu, K. Yamamoto, S. Yokoyama, An analysis of the structural, thermal and optical characteristics as well as the electrical resistivity of tert-butyldiphenylsilyl substituted poly(norbornene-dicarboximide)s, Polymer (Guildf). 56 (2015) 189–198, https://doi.org/10.1016/j.polymer.2014.11.043.

[21] T.H. Tran, C.T. Nguyen, L. Gonzalez-Fajardo, D. Hargrove, D. Song, P. Deshmukh, L. Mahajan, D. Ndaya, L. Lai, R.M. Kasi, X. Lu, Long circulating self-assembled nanoparticles from cholesterol-containing brush-like block copolymers for improved drug delivery to tumors, Biomacromolecules 15 (2014) 4363–4375, https://doi.org/10.1021/bm5013822.

[22] H. jing Han, S. Zhang, R. yi Sun, J. hua Wu, M. ran Xie, X. juan Liao, Photocrosslinkable polynorbornene-based block copolymers with enhanced dielectric and thermal properties, Chinese J. Polym. Sci. (English Ed. 34 (2016) 378–389. https://doi.org/10.1007/s10118-016-1753-0.

[23] T. Pelras, C.S. Mahon, M. Müllner, Synthesis and applications of compartmentalised molecular polymer brushes, Angew. Chemie - Int. Ed. 57 (2018) 6982–6994, https://doi.org/10.1002/anie.201711878.

[24] M.F. Radwan, M.F. Aly, A.M. Spring, A.A. Abuelwafa, Enhancing optical and electrical properties of acetophenone azo anthrone dye thin films T hrough cyclodextrin inclusion complex, J. Inorg. Organomet. Polym Mater. 35 (2025) 4118–4133, https://doi.org/10.1007/s10904-024-03515-4.

[25] K.S. Sadovnikov, I.V. Nazarov, V.A. Zhigarev, A.A. Danshina, I.S. Makarov, M. V. Bermeshev, Cross-linked metathesis polynorbornenes based on nadimides bearing hydrocarbon substituents: synthesis and physicochemical properties, Polymers (Basel). 16 (2024), https://doi.org/10.3390/polym16182671.

[26] I.V. Nazarov, A.P. Khrychikova, E.I. Medentseva, E.V. Bermesheva, I.L. Borisov, A. A. Yushkin, A.V. Volkov, A.I. Wozniak, D.I. Petukhov, M.A. Topchiy, A. F. Asachenko, X.-K. Ren, M.V. Bermeshev, CO2-selective vinyl-addition polymers from nadimides: synthesis and performance for membrane gas separation, J. Memb. Sci. 677 (2023) 121624, https://doi.org/10.1016/j.memsci.2023.121624.

[27] M.A. Zotkin, D.A. Alentiev, R.S. Borisov, A.A. Kozlova, I.L. Borisov, M.G. Shalygin, M.V. Bermeshev, Polynorbornenes with carbocyclic substituents: a perspective approach to highly permeable gas separation membranes, J. Memb. Sci. 702 (2024) 122786, https://doi.org/10.1016/j.memsci.2024.122786.

[28] O.A. Adzhieva, R.Y. Nikiforov, M.L. Gringolts, N.A. Belov, M.P. Filatova, Y. I. Denisova, Y.V. Kudryavtsev, Synthesis and gas separation properties of metathesis poly(5-perfluorobutyl-2-norbornene), Polym. Sci., Ser. A 64 (2022) 424–433, https://doi.org/10.1134/S0965545X22700262.

[29] V.A. Zhigarev, A.A. Morontsev, R.Y. Nikiforov, M.L. Gringolts, N.A. Belov, N. G. Komalenkova, V.G. Lakhtin, E.S. Finkelshtein, Synthesis and gas-separation properties of new silacyclopentane-containing polynorbornenes, Polym. Sci., Ser. C 61 (2019) 107–119, https://doi.org/10.1134/S1811238219010181.

[30] J. Vargas, A.A. Santiago, J.A. Cruz-Morales, M.A. Tlenkopatchev, T. De Lys, M. Lõpez-González, E. Riande, Gas transport properties of hydrogenated and fluorinated polynorbornene dicarboximides, Macromol. Chem. Phys. 214 (2013) 2607–2615, https://doi.org/10.1002/macp.201300401.

[31] M.Z. Basyouni, K. Nomura, Y. Goroumaru, M.F. Radwan, M.E. Abdu, A.M. Spring, Controlled synthesis of PPV oligomers by ROMP: impact on optical, structural, and thermal properties, Chem. Pap. 79 (2025) 4687–4700, https://doi.org/10.1007/s11696-025-04091-8.
[32] A.M. Spring, F. Qiu, J. Hong, A. Bannaron, X. Cheng, S. Yokoyama, Adamantyl and carbazole containing trans-poly(norbornene-dicarboximide)s as electro-optic chromophore hosts, Polymer (Guildf). 172 (2019) 382–390, https://doi.org/10.1016/j.polymer.2019.04.015.
[33] M.F. Radwan, M.Z. Basyouni, M.E. Abdu, A.G. Taha, P. Xia, A.M. Spring, Unlocking the potential of poly(norbornene-dicarboximides): synthesis, applications, and future prospects, Int. Exch. Innov. Conf. Eng. Sci. 10 (2024) 1114–1121, https://doi.org/10.5109/7323397.
[34] S. Kumar, S. Supriya, M. Kar, Enhancement of dielectric constant in polymer-ceramic nanocomposite for flexible electronics and energy storage applications, Compos. Sci. Technol. 157 (2018) 48–56, https://doi.org/10.1016/j.compscitech.2018.01.025.
[35] D.H.N. Santos, G.H.C. Masson, E.A. Silva, R.J.G. Rubira, O.R. Nascimento, K. Bernardo-Gusmão, B.S. Lima-Neto, B.E. Goi, V.P. Carvalho-Jr, Tandem ROMP/Vinyl-addition polymerization of norbornene catalyzed by a Ru/Ni heterobimetallic complex, J. Polym. Sci. 63 (2025) 2146–2157, https://doi.org/10.1002/pol.20241092.
[36] X. Wang, Y.L. Jeong, C. Love, H.A. Stretz, G.E. Stein, B.K. Long, Design, synthesis, and characterization of vinyl-addition polynorbornenes with tunable thermal properties, Polym. Chem. 12 (2021) 5831–5841, https://doi.org/10.1039/d1py01050f.
[37] E.I. Medentseva, A.P. Khrychikova, E.V. Bermesheva, I.L. Borisov, D.I. Petukhov, G. O. Karpov, A.A. Morontsev, O.V. Nesterova, M.V. Bermeshev, CO_2-separation performance of vinyl-addition polynorbornenes with ester functionalities, J. Memb. Sci. 705 (2024) 122916, https://doi.org/10.1016/j.memsci.2024.122916.
[38] I. Pérez-Ortega, A.C. Albéniz, Vinylic addition poly(norbornene-co-alkenylnorbornenes) synthesized with benzylic palladium catalysts: materials for manifold functionalization, Polym. Chem. 13 (2022) 4154–4161, https://doi.org/10.1039/d2py00643j.
[39] E.C. Kim, M.J. Kim, L.N. Thi Ho, W. Lee, J.W. Ka, D.G. Kim, T.J. Shin, K.M. Huh, S. Park, Y.S. Kim, Synthesis of vinyl-addition polynorbornene copolymers bearing pendant n-alkyl chains and systematic investigation of their Properties, Macromolecules 54 (2021) 6762–6771, https://doi.org/10.1021/acs.macromol.1c00858.
[40] K.H. Park, R.J. Twieg, R. Ravikiran, L.F. Rhodes, R.A. Shick, D. Yankelevich, A. Knoesen, Synthesis and nonlinear-optical properties of vinyl-addition poly (norbornene)s, Macromolecules 37 (2004) 5163–5178, https://doi.org/10.1021/ma040044i.
[41] A.H. Tantawy, H.I. Mohamed, A.A. Khalil, K.A. Hebash, M.Z. Basyouni, Novel bioactive imidazole-containing polymeric surfactants as petroleum-collecting and dispersing agents: Synthesis and surface-active properties, J. Mol. Liq. 236 (2017) 376–384, https://doi.org/10.1016/j.molliq.2017.04.040.
[42] A.M. Spring, F. Qiu, S. Yokoyama, High stability poly(N-adamantyl-exo-norbornene-5,6-dicarboximide) and phenyl vinylene thiophene electro-optic host-guest system, Eur. Polym. J. 84 (2016) 89–99, https://doi.org/10.1016/j.eurpolymj.2016.09.012.
[43] S. Park, M.C. Choi, H.J. Cho, W.J. Shin, W.B. Jang, G.S. Chae, C.S. Ha, Syntheses and characterization of functionalized polynorbornene dicarboximides for flexible substrates, Polym. Adv. Technol. 24 (2013) 249–257, https://doi.org/10.1002/pat.3077.
[44] A. Pineda Contreras, M.A. Tlenkopatchev, M. Del Mar López-González, E. Riande, Synthesis and gas transport properties of new high glass transition temperature ring-opened polynorbornenes, Macromolecules 35 (2002) 4677–4684, https://doi.org/10.1021/ma011959p.
[45] B. Liu, Y. Li, A.S. Mathews, Y. Wang, W. Yan, S. Abraham, C.S. Ha, D.W. Park, I. Kim, Synthesis of vinyl-type functionalized polynorbornenes with cyclic pendant imide side groups by using palladium-based catalyst for low dielectric constant materials, React. Funct. Polym. 68 (2008) 1619–1624, https://doi.org/10.1016/j.reactfunctpolym.2008.09.003.
[46] H.I. Mohamed, M.Z. Basyouni, A.A. Khalil, K.A. Hebash, A.H. Tantawy, Petroleum-dispersing and antimicrobial activity of newly synthesized polymeric surfactants tethering tetrachlorophthalimide moiety, J. Iran. Chem. Soc. 18 (2021) 265–274, https://doi.org/10.1007/s13738-020-02023-9.
[47] C.B. Braga, R.A. Pilli, C. Ornelas, M. Weck, Near-infrared fluorescent micelles from poly(norbornene) brush triblock copolymers for nanotheranostics, Biomacromolecules 22 (2021) 5290–5306, https://doi.org/10.1021/acs.biomac.1c01196.
[48] C.J. Lin, Y.H. Lin, T.C. Chiang, C.Y. Yu, Synthesis of the polymers containing norbornene and tetraphenylethene by ring-opening metathesis polymerization and their structural characterization, aggregation-induced emission and aniline detection, Polymer (guildf). 260 (2022) 125374, https://doi.org/10.1016/j.polymer.2022.125374.
[49] J. Wu, Y. Fu, W. Liu, X. Liao, M. Xie, R. Sun, Synthesis and properties of tricarbazole-functionalized poly(norbornene-dicarboximide), Eur. Polym. J. 76 (2016) 110–121, https://doi.org/10.1016/j.eurpolymj.2016.01.037.
[50] H. Tetsuka, M. Hagiwara, S. Kaita, Addition-type poly(norbornene)s with siloxane substituents: synthesis, properties and nanoporous membrane, Polym. J. 43 (2011) 97–100, https://doi.org/10.1038/pj.2010.99.
[51] M.F. Radwan, E.E. Elboray, H.M. Dardeer, Y. Kobayashi, T. Furuta, S. Hamada, T. Dohi, M.F. Aly, 1,3-Dipolar cycloaddition of 3-chromonyl-substituted glycine imino esters with arylidenes and in situ diastereodivergent via retrocycloaddition, Chem. - an Asian J. 18 (2023), https://doi.org/10.1002/asia.202300215.
[52] C. Plessis, G. Arzamendi, J.M. Alberdi, M. Agnely, J.R. Leiza, J.M. Asua, Intramolecular chain transfer to polymer in the emulsion polymerization of 2-ethylhexyl acrylate, Macromolecules 34 (2001) 6138–6143, https://doi.org/10.1021/ma0018190.
[53] S.L. Fronk, M. Wang, M. Ford, J. Coughlin, C.K. Mai, G.C. Bazan, Effect of chiral 2-ethylhexyl side chains on chiroptical properties of the narrow bandgap conjugated polymers PCPDTBT and PCDTPT, Chem. Sci. 7 (2016) 5313–5321, https://doi.org/10.1039/c6sc00908e.
[54] C.R.G. Grenier, S.J. George, T.J. Joncheray, E.W. Meijer, J.R. Reynolds, Chiral ethylhexyl substituents for optically active aggregates of π-conjugated polymers, J. Am. Chem. Soc. 129 (2007) 10694–10699, https://doi.org/10.1021/ja068461t.
[55] M.Z. Basyouni, M.F. Radwan, M.E. Abdu, A.M. Spring, Synthesis, characterization, and optical properties of carbazole-functionalized poly(norbornene-dicarboximide) by ROMP, Evergreen 11 (2024) 207–213, https://doi.org/10.5109/7172257.
[56] M.F. Radwan, M.E. Abdu, M.M. Elkady, M.Z. Basyouni, A.M. Spring, Living ROMP of N-phenothiazinyl norbornene-dicarboximide homopolymer: synthesis, characterization, and physical behavior insights, Polymer 321 (2025) 128115, https://doi.org/10.1016/j.polymer.2025.128115.
[57] J. Pozuelo, M. López-González, M. Tlenkopatchev, E. Saiz, E. Riande, Simulations of gas transport in membranes based on polynorbornenes functionalized with substituted imide side groups, J. Memb. Sci. 310 (2008) 474–483, https://doi.org/10.1016/j.memsci.2007.11.019.
[58] A.A. Santiago, J. Vargas, J. Cruz-gómez, M.A. Tlenkopatchev, R. Gaviño, M. López-gonzález, E. Riande, Synthesis and ionic transport of sulfonated ring-opened polynorbornene based copolymers, Polymer (Guildf). 52 (2011) 4208–4220, https://doi.org/10.1016/j.polymer.2011.07.030.
[59] A.M. Spring, F. Yu, F. Qiu, K. Yamamoto, S. Yokoyama, The preparation of well-controlled poly(N-cyclohexyl-exo-norbornene-5, 6-dicarboximide) polymers, Polym. J. 46 (2014) 576–583, https://doi.org/10.1038/pj.2014.26.
[60] M.F. Radwan, M.E. Abdu, M.Z. Basyouni, M.M. Elkady, M.M. Zohair, K. Shimizu, A. M. Spring, From monomer design to multifunctional polymers via controlled ROMP: novel indole-functionalized norbornene dicarboximide copolymers with enhanced thermal, optical, and antibacterial properties, Macromolecules 58 (2025) 8007–8031, https://doi.org/10.1021/acs.macromol.5c01339.
[61] F. Yu, A.M. Spring, L. Li, F. Qiu, K. Yamamoto, D. Maeda, M. Ozawa, K. Odoi, S. Yokoyama, An enhanced host-guest electro-optical polymer system using poly (norbornene-dicarboximides) via ROMP, J. Polym. Sci., Part A: Polym. Chem. 51 (2013) 1278–1284, https://doi.org/10.1002/pola.26505.
[62] C.W. Bielawski, R.H. Grubbs, Living ring-opening metathesis polymerization, Prog. Polym. Sci. 32 (2007) 1–29, https://doi.org/10.1016/j.progpolymsci.2006.08.006.
[63] Y. Ma, Z. Kang, Q. Zheng, Recent advances in wide bandgap semiconducting polymers for polymer solar cells, J. Mater. Chem. A 5 (2017) 1860–1872, https://doi.org/10.1039/c6ta09325f.
[64] A.H.A. Darwesh, S.B. Aziz, S.A. Hussen, Insights into optical band gap identification in polymer composite films based on PVA with enhanced optical properties: Structural and optical characteristics, Opt. Mater. (Amst). 133 (2022) 113007, https://doi.org/10.1016/j.optmat.2022.113007.
[65] L. Zhang, B. Feng, S. Pang, H. Xin, K. Li, Y. Jin, Synthesis and performance study of nonionic photoacid generators based on Norbornene-imide, J. Mol. Struct. 1304 (2024) 137653, https://doi.org/10.1016/j.molstruc.2024.137653.
[66] P. Wang, J.A. Linares-Pastén, B. Zhang, Synthesis, molecular docking simulation, and enzymatic degradation of AB-type indole-based polyesters with improved thermal properties, Biomacromolecules 21 (2020) 1078–1090, https://doi.org/10.1021/acs.biomac.9b01399.
[67] Y. Jia, A.M. Spring, F. Qiu, F. Yu, K. Yamamoto, I. Aoki, A. Otomo, S. Yokoyama, Electro-optic properties of a bi-chromophore norbornene polymer brush system, Jpn. J. Appl. Phys. 53 (2014) 01AF04, https://doi.org/10.7567/JJAP.53.01AF04.
[68] K.H. Yoon, K.O. Kim, M. Schaefer, D.Y. Yoon, Synthesis and characterization of hydrogenated poly(norbornene endo-dicarboximide)s prepared by ring opening metathesis polymerization, Polymer (guildf). 53 (2012) 2290–2297, https://doi.org/10.1016/j.polymer.2012.02.047.
[69] B. Bingöl, A. Kroeger, P. Jannasch, Well-defined phosphonated homo- and copolymers via direct ring opening metathesis polymerization, Polymer (guildf). 54 (2013) 6676–6688, https://doi.org/10.1016/j.polymer.2013.10.018.
[70] R. Xie, A.R. Weisen, Y. Lee, M.A. Aplan, A.M. Fenton, A.E. Masucci, F. Kempe, M. Sommer, C.W. Pester, R.H. Colby, E.D. Gomez, Glass transition temperature from the chemical structure of conjugated polymers, Nat. Commun. 11 (2020) 4–11, https://doi.org/10.1038/s41467-020-14656-8.
[71] W. Xia, J. Song, D.D. Hsu, S. Keten, Side-group size effects on interfaces and glass formation in supported polymer thin films, J. Chem. Phys. 146 (2017) 203311, https://doi.org/10.1063/1.4976702.
[72] A.P. Contreras, A.M. Cerda, M.A. Tlenkopatchev, Synthesis of high-Tg polymers by ring-opening metathesis polymerization of N-cycloalkylnorbornene dicarboximide, Macromol. Chem. Phys. 203 (2002) 1811–1818, https://doi.org/10.1002/1521-3935(200208)203:12<1811::AID-MACP1811>3.0.CO;2-J.
[73] P. Wang, C.R. Arza, B. Zhang, Indole as a new sustainable aromatic unit for high quality biopolyesters, Polym. Chem. 9 (2018) 4706–4710, https://doi.org/10.1039/c8py00962g.